Dalton Transactions

Accepted Manuscript

ROYAL SOCIETY OF CHEMISTRY

www.rsc.org/dalton

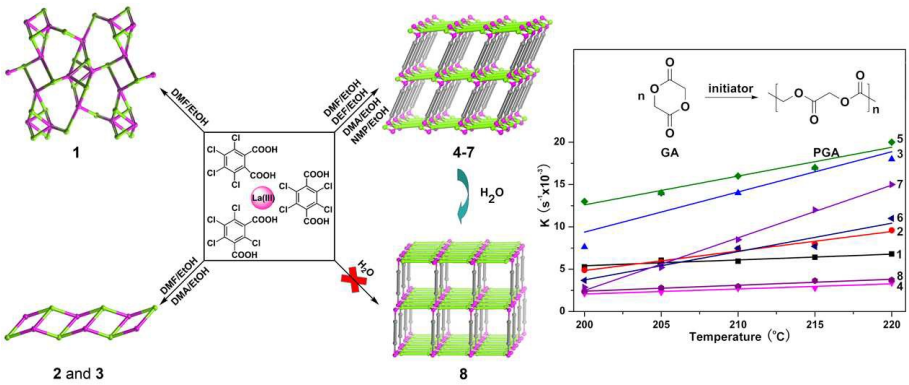

Eight La(III) coordination polymers with topological diversity were prepared from isomeric perchlorinated benzenedicarboxylate ligands. Water-induced structural transformation was reported. All complexes show catalytic activity towards the ring-opening polymerization of glycolide.

ARTICLE Journal Name

Assembly of 1D, 2D and 3D lanthanum(III) coordination polymers with perchlorinated benzenedicarboxylates: positional isomeric effect, structural transformation and ring-opening polymerisation of glycolide

Received 00th January 20xx,
Accepted 00th January 20xx

DOI: 10.1039/x0xx00000x

www.rsc.org/

Sheng-Chun Chen,[a,b] An-Qi Dai,[b] Kun-Lin Huang,*[c] Zhi-Hui Zhang,[b] Ai-Jun Cui,[b] Ming-Yang He*[b] and Qun Chen*[a,b]

Utilizing a series of positional isomers of tetrachlorinated benzenedicarboxylic acid ligands, seven La(III)-based coordination polymers were solvothermally synthesized and structurally characterized. Their structural dimensionalities varying from 1D double chains, to 2D 3,4,5-connected network, to 3D 6-connected **pcu** topological nets are only governed by the positions of carboxyl groups on the tetrachlorinated benzene ring. A comprehensive analysis and comparison reveals that the size of the carbonyl solvent molecules (DMF, DEF, DMA, and NMP) can affect the coordination geometries around the La(III) ions, the coordination modes of carboxylate groups, the packing arrangements, and the void volumes of overall crystal lattices. One as-synthesized framework further shows an unprecedented structural transformation from 3D 6-connected network to 3D 4,5-connected net through the dissolution and reformation pathway in water, suggesting that these easily hydrolyzed lanthanide complexes may server as precursors to produce new high-dimensional frameworks. The bulk solvent-free melt polymerisation of glycolide utilizing these La(III) complexes as initiators has been reported herein for the first time. All complexes were found to promot the polymerization of glycolide over a temperature range of 200 to 220 °C, producing poly(glycolic acid) (PGA) with molecular weight up to 93280. Under the same experimental conditions, the different catalytic activities for these complexes may result from their structural discrepancy.

Introduction

The rational design and construction of new functional coordination polymers (CPs) have gained particular attention in recent years, mainly because of their structural diversities and potential applications as functional materials in many useful areas.[1–8] Despite these remarkable progresses, however, to date, controlling the structural topology and dimensionality of the target compounds still remains a challenge in crystal engineering. It has been recognized that the formation of coordination architectures mainly depend on the coordination geometry of metal ions and the nature of organic ligands,[9–12] and the self-assembly processes are also frequently modulated by various synthesis conditions such as reaction temperature,[13] solvent system,[14] pH value,[15] and so on. Among these factors, the choice of organic ligands is very important in determining the ultimate topology of the coordination solids. In this aspect, systematic tuning of structural topologies and properties of CPs has been successfully established and developed by the utilization of positional isomeric effect, spacer effect, and substituent effect.[16–19] For example, a few set of isomeric aromatic dicarboxylate anions such as benenedicarboxylates,[20–22] biphenyldicarboxylates,[23] phenylenediacetates,[24–27] and pyrdinedicarboxylates,[28–30] were used to connect the transition metal ions for the fabrication of diverse coordination networks with or without the auxiliary ligands. In contrast to transition-metal-carboxylate CPs, lanthanide-based networks manipulated by positional isomeric aromatic dicarboxylates, to our knowledge, have rarely been reported.[22] The most important reason may be that lanthanide ions generally possess variable and high coordination numbers as well as flexible coordination geometry, which make it difficult to control the synthetic reactions and thereby the structures of the products formed.

More importantly, many of lanthanide complexes have recently exhibited excellent catalytic properties for organic transformations and polymerization reactions.[31] For instance, lanthanide complexes have proven to be efficient initiators for the ring-opening polymerization (ROP) of cyclic monomers such as lactide and *ε*-caprolactone.[32–36] Since lanthanide-metal complexes promote the ROP of cyclic esters via a similar coordination-insertion mechanism to that of various alkali- and transition-metal complexes,[37–39] it is of great importance to further understand the relationship between the structure and its catalytic activity of lanthanide complexes. Most of the research efforts in this area have so far been focused on the design and synthesis of lanthanide complexes having discrete structures. In recent years, many infinite lanthanide-based CPs, especially polymeric metal carboxylates, are currently evaluated as heterogeneous catalysts for a wide range of organic transformations,[40–43] however, to the best of our knowledge, utilizing them as homogeneous initiators in the ROP of cyclic esters has been scarcely explored.

Sparked by the above points and our recent studies on the assembly of CPs with perhalogenated benzenedicarboxylate

[a] School of Chemical Engineering, Nanjing University of Science and Technology, Nanjing 20094, PR China. E-mail:chenqunjpu@yahoo.com
[b] School of Petrochemical Engineering, Jiangsu Key Laboratory of Advanced Catalytic Materials and Technology, Changzhou University, Changzhou 213164, PR China.
[c] College of Chemistry, Chongqing Normal University, Chongqing 401331, PR China. E-mail: kunlin@cqnu.edu.cn.

†Electronic Supplementary Information (ESI) available: [details of any supplementary information available should be included here]. See DOI: 10.1039/x0xx00000x

ligands,[44–48] we sought to systematically investigate the role of three positional isomers (1,2-; 1,3-; 1,4-) of tetrachlorinated benzenedicarboxylate (tcbdc) ligands (Scheme 1) in association with the assembly and structural variability as well as catalytic properties of the lanthanide(III)-based CPs. Herein, we report a series of La(III)-based CPs: $\{[La_2(1,2\text{-tcbdc})_3(H_2O)_4]\cdot EtOH\}_n$ (**1**), $[La(1,3\text{-tcbdc})(OAc)(DMF)_2(H_2O)]_n$ (**2**), $[La(1,3\text{-tcbdc})(OAc)(DMA)_2(H_2O)]_n$ (**3**), $[La(1,4\text{-tcbdc})_{1.5}(DMF)(H_2O)_3]_n$ (**4**), $[La(1,4\text{-tcbdc})_{1.5}(DEF)(EtOH)(H_2O)]_n$ (**5**), $\{[La(1,4\text{-tcbdc})_{1.5}(DMA)_2(H_2O)]\cdot DMA\}_n$ (**6**) $\{[La(1,4\text{-tcbdc})_{1.5}(NMP)_2(H_2O)]\cdot NMP\}_n$ (**7**), and $\{[La(1,4\text{-tcbdc})_{1.5}(H_2O)]\cdot 3H_2O\}_n$ (**8**) (DMF = N,N-dimethylformamide, DMA = N,N-dimethylacetamide, DEF = N,N-diethylformamide, and NMP = N-methyl-2-pyrrolidone), where **1–7** were synthesized by using three structural isomers of H_2tcbdc ligands and changing the solvent systems under solvothermal conditions, while **8** was obtained upon hydrolysis and recrystallization of **4** (Scheme 2). Their diverse topological structures with 1D double chain, 2D sheet and 3D networks can be controlled by the positions of the carboxyl groups on tcbdc backbones, where an unusual 3D structural transformation from **4** to **8** was also observed. For the first time, the solid-state bulk polymerization of glycolide utilizing the eight lanthanide complexes as initiators has been carried out. The results show that all complexes exhibits substantial catalytic activity for the ring-opening polymerization of glycolide to produce poly(glycolic acid) (PGA) with high molecular weight, and the difference in reactivity may be attributed to the structural diversity of these complexes formed.

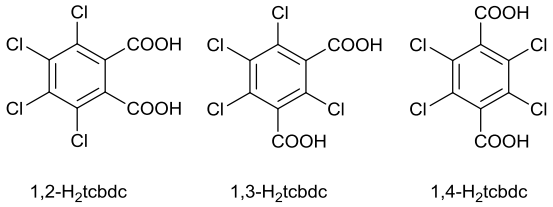

Scheme 1 Positional isomeric H_2tcbdc ligands used in this work.

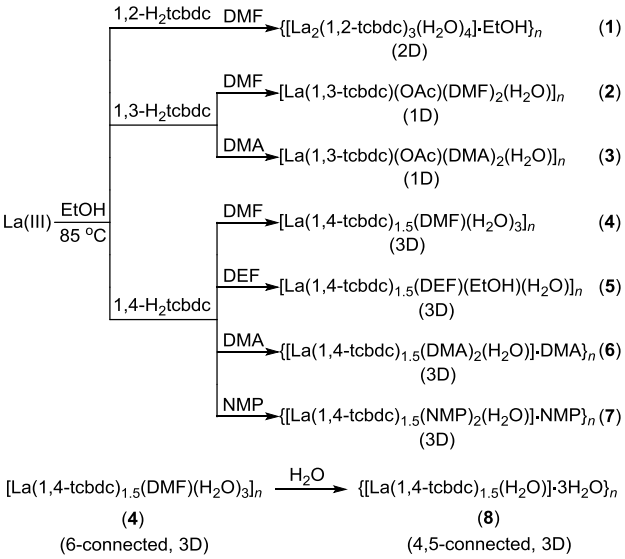

Scheme 2 The outline of complexes **1–8**.

Experimental

Materials and methods

All reagents and solvents for synthesis and analysis were commercially available and used as received. The Fourier transform (FT) IR spectra (KBr pellets) were recorded on a Nicolet ESP 460 FT-IR spectrometer. Elemental analyses of carbon, hydrogen and nitrogen were performed on a PE-2400II (Perkin-Elmer) analyzer. Powder X-ray diffraction (PXRD) patterns were recorded on a Rigaku D/Max-2500 diffractometer at 40 kV and 100 mA for a Cu-target tube (λ = 1.5406 Å). The calculated PXRD patterns were obtained from the single-crystal diffraction data using the PLATON software.[49] Thermogravimetric (TG) analyses were performed on a SDT 600 instrument from room temperature to 800 °C with a heating rate of 10 °C min^{-1} under nitrogen stream.

Syntheses of complexes 1–8

$\{[La_2(1,2\text{-tcbdc})_3(H_2O)_4]\cdot EtOH\}_n$ (**1**). A mixture containing $La(NO_3)_3\cdot 6H_2O$ (86.6 mg, 0.2 mmol), 1,2-H_2tcbdc (60.8 mg, 0.2 mmol), NaOH (16.0 mg, 0.4 mmol), ethanol (3 mL), water (1 mL) and DMF (3 mL) was sealed in a Teflon-lined stainless steel vessel (15 mL), which was heated to 85 °C and held at that temperature for 72 h, then cooled to 30 °C at a rate of 3 °C h^{-1}. Colorless block crystals of **1** were obtained and washed with ethanol. Isolated yield: ~42% based on 1,2-H_2tcbdc. Anal. calcd for $C_{26}H_{14}Cl_{12}La_2O_{17}$: C, 23.99; H, 1.08%. Found: C, 24.47; H, 1.09%. IR (cm^{-1}): 3397 br, 2964 m, 2928 m, 1664 s, 1586 s,1524 s, 1428 s, 1344 s, 1212 m, 1131 m, 1101 w, 936 w, 919 m, 832 m, 666 m, 650 m, 619 m.

$[La(1,3\text{-tcbdc})(OAc)(DMF)_2(H_2O)]_n$ (**2**). The synthetic procedure of **2** was similar to that described for **1**, except that $La(OAc)_3\cdot 5H_2O$ (63.2 mg, 0.2 mmol) and 1,3-H_2tcbdc (60.8 mg, 0.2 mmol) were used instead of $La(NO_3)_3\cdot 6H_2O$ and 1,2-H_2tcbdc. Isolated yield: ~68% based on 1,3-H_2tcbdc. Anal. calcd for $C_{16}H_{19}Cl_4LaN_2O_9$: C, 28.94; H, 2.89; N, 4.22%. Found: C, 28.51; H, 2.89; N, 4.37%. IR (cm^{-1}): 3527 m, 3403 br, 2983 m, 2935 m, 2848 m, 1584 s, 1446 s, 1345 s, 1326 s, 1108 w, 1056 m, 1016 s, 934 m, 846 w, 775 s, 730 s, 659 s, 614 s, 471 m.

$[La(1,3\text{-tcbdc})(OAc)(DMA)_2(H_2O)]_n$ (**3**). The synthetic procedure of **3** was similar to that described for **2**, except that DMA (3 mL) was used instead of DMF. Isolated yield: ~53% based on 1,3-H_2tcbdc. Anal. calcd for $C_{18}H_{23}Cl_4LaN_2O_9$: C, 31.24; H, 3.35; N, 4.05%. Found: C, 31.83; H, 3.67; N, 4.12%. IR (cm^{-1}): 3528 m, 3272 br, 2981 m, 2936 m, 1659 s, 1609 s, 1548, 1451 s, 1405 s, 1338 s, 1262 m, 1192 m, 1056 m, 1020 s, 942 m, 892 w, 730 s, 659 s, 614 s, 529 m, 478 m.

$[La(1,4\text{-tcbdc})_{1.5}(DMF)(H_2O)_3]_n$ (**4**). The synthetic procedure of **4** was similar to that described for **1**, except that 1,4-H_2tcbdc (60.8 mg, 0.2 mmol) was used instead of 1,2-H_2tcbdc. Isolated yield:

~76% based on 1,4-H_2tcbdc. Anal. calcd for $C_{15}H_{13}Cl_6LaNO_{10}$: C, 25.06; H, 1.83; N, 1.95%. Found: C, 24.92; H, 1.81; N, 2.01%. IR (cm^{-1}): 3631 s, 3146 br, 2974 s, 2944 s, 1653 s, 1596 s, 1433 s, 1405 s, 1332 s, 1248 s, 1156 m, 1107 s, 1060 m, 1018 s, 936 w, 863 s, 776 s, 674 s, 612 s.

[La(1,4-tcbdc)$_{1.5}$(DEF)(EtOH)(H_2O)]$_n$ (**5**). The synthetic procedure of **5** was similar to that described for **4**, except that DEF (3 mL) was used instead of DMF. Isolated yield: ~65% based on 1,4-H_2tcbdc. Anal. calcd for $C_{19}H_{19}Cl_6LaNO_9$: C, 30.15; H, 2.53; N, 1.85%. Found: C, 32.05; H, 2.49; N, 1.83%. IR (cm^{-1}): 3593 m, 3501 br, 2980 m, 2938 m, 1632 s, 1598 s, 1552 s, 1447 s, 1408 s, 1342 s, 1261 m, 1125 m, 1152 s, 1123 s, 1057 m, 1018 m, 944 m, 832 m, 753 s, 655 s, 609 s, 499 m.

{[La(1,4-tcbdc)$_{1.5}$(DMA)$_2$(H_2O)]·DMA}$_n$ (**6**). The synthetic procedure of **6** was similar to that described for **4**, except that DMA (3 mL) was used instead of DMF. Isolated yield: ~68% based on 1,4-H_2tcbdc. Anal. calcd for $C_{24}H_{29}Cl_6LaN_3O_{10}$: C, 33.09; H, 3.36; N, 4.82%. Found: C, 32.83; H, 3.38; N, 4.77%. IR (cm^{-1}): 3636 m, 3338 br, 2940 m, 2823 m, 1589 s, 1514 s, 1425 s, 1408 s, 1332 s, 1261 s, 1188 m, 1152 m, 1117 m, 1060 m, 1026 s, 1026 s, 968 m, 862 m, 750 s, 707 s, 611 s, 485 s.

{[La(1,4-tcbdc)$_{1.5}$(NMP)$_2$(H_2O)]·NMP}$_n$ (**7**). The synthetic procedure of **7** was similar to that described for **4**, except that NMP (3 mL) was used instead of DMF. Isolated yield: ~52% based on 1,4-H_2tcbdc. Anal. calcd for $C_{27}H_{29}Cl_6LaN_3O_{10}$: C, 35.75; H, 3.22; N, 4.63%. Found: C, 36.13; H, 3.18; N, 4.72%. IR (cm^{-1}): 3648 w, 3454 br, 2964 m, 2933 m, 2880 m, 1678 s, 1636 s, 1559 s, 1616 s, 1476 m, 1409 s, 1335 s, 1260 m, 1152 m, 1116 s, 1073 m, 1020 m, 929 w, 861 m, 750 m, 669 m, 609 s, 468 m.

{[La(1,4-tcbdc)$_{1.5}$(H_2O)]·3H_2O}$_n$ (**8**). Complex **4** (1.438 g, 2.0 mmol) was dissolved in 8 mL deionized water. Upon slow evaporation of the solution over five weeks, colorless needle-like crystals of **8** were produced. Isolated yield: ~76% based on 4. Anal. calcd for $C_{12}H_8Cl_6LaO_{10}$: C, 21.71; H, 1.21%. Found: C, 22.45; H, 1.43%. IR (cm^{-1}): 3685 m, 3569 m, 3405 br, 2973 m, 1648 s, 1554 s, 1439 s, 1339 s, 1250 m, 1131 m, 1124 m, 1090 w, 1048 m, 930 w, 866 s, 842 m, 803 m, 755 m, 701 m, 626 s.

Glycolide polymerization procedure

The isothermal experiments of glycolide polymerization were performed on a Perkin-Elmer's differential scanning calorimeter (DSC) running under a nitrogen atmosphere (50 mL min^{-1}), and the DSC data were analyzed by Pyris Kinetic Analysis software. Indium (156.6 °C) was employed as a standard sample for the calibration of temperature and heat. The necessary quantities of lanthanide(III) complex and glycolide were mixed, and a suitable amount of sample was taken for DSC measurements. The typical sample weight for DSC measurement was 5 mg. The experiments were run in aluminum pans. The mixture reaction samples were heated at a heating rate of 600 °C min^{-1} to the temperature in the range of 200–230 °C, and then kept for 15 min.

Molecular weights (M_n and M_w) and molecular-weight dispersities (M_w/M_n) were measured by gel permeation chromatography (GPC). The measurements were performed at 40 °C on a Waters 1525 binary system equipped with a Waters 2414 Refractive Index (RI) detector and a Waters 2487 dual λ absorbtion (UV, λ_{abs} = 220 nm) detector. In the case of the analyses performed using a solution of sodium trifluoroacetate (0.68 g, 5 mmol) in 1,1,1,3,3,3-hexafluoro-2-propanol (1000 mL) as eluent at a flow rate of 0.6 mL min^{-1}, a system of four Styragel HR columns (7.8 × 300 mm; range 10^3–10^6 Å) was employed. The molecular weights were calculated with respect to poly(methyl methacrylate) (PMMA) standards (M_n ranging from 7000 to 200000).

X-Ray crystallography

Single-crystal X-ray diffraction measurements of **1–8** were performed on a Bruker APEX II CCD diffractometer at the ambient temperature with Mo Kα radiation (λ = 0.71073 Å). In each case, a semiempirical absorption correction was applied using SADABS,[50] and the program SAINT was used for integration of the diffraction profiles.[51] The structures were solved by direct methods with SHELXS and refined by full-matrix least-squares on F^2 with the SHELXL program of the SHELXTL package.[52] All non-hydrogen atoms were refined anisotropically. C–bound hydrogen atoms were placed in geometrically calculated positions by using a riding model. O–bound hydrogen atoms were localized by difference Fourier maps and refined in subsequent refinement cycles. The SQUEEZE[53] option of PLATON was used to treat regions of diffuse electron density that could not be appropriately modeled for **1** and **8** and remove their contribution to the overall intensity data. The squeezed solvents were assigned as ethanol in **1** and water in **8** because the original electron peaks seemed to resemble these solvents. The coordinated EtOH and DEF molecules in **5** are severely disordered. Notably, one DEF molecule was disordered over two parts and refined with equal occupancy factors. Another DMF molecule was found to coexist with EtOH, the occupancy ratio was refined to 0.5/0.5. The final chemical formulas of **1** and **8** were obtained from crystal data combined with the results of elemental and thermogravimetric analysis. The details of crystallographic parameters, data collection and refinements for the complexes are listed in Table 1.

Results and discussion

Synthesis and general characterization

In order to explore the role of isomeric H_2tcbdc ligands on assembly, structural variability and properties of the lanthanide(III)-based CPs, complexes **1–7** were obtained under solvothermal conditions. This method is different from that of our previously reported complexes based on H_2tcbdc,[41–43] which were obtained by evaporating the reaction solutions at room temperature. In the present study, our first attempts to react the three isomers of H_2tcbdc with various lanthanide nitrate and acetate salts in the mixed DMF/EtOH solvent by solvothermal methods gave only the crystals of La(III)-based compounds of **1**, **2** and **4**. It was found that **1** based on 1,2-H_2tcbdc and **2** based on 1,3-H_2tcbdc as well as **4** based on 1,4-H_2tcbdc display 2D, 1D, and 3D networks, respectively.

Table 1 Crystal data and structure refinement for complexes **1–8**

	1	**2**	**3**	**4**	**5**	**6**	**7**	**8**
Formula	$C_{26}H_{14}Cl_{12}La_2O_{17}$	$C_{16}H_{19}Cl_4LaN_2O_9$	$C_{18}H_{23}Cl_4LaN_2O_9$	$C_{15}H_{13}Cl_6LaNO_{10}$	$C_{19}H_{19}Cl_6La_2NO_9$	$C_{24}H_{29}Cl_6LaN_3O_{10}$	$C_{27}H_{29}Cl_6LaN_3O_{10}$	$C_{12}H_8Cl_6LaO_{10}$
Formula weight	1301.59	664.04	692.09	718.87	756.96	871.11	907.14	663.79
Crystal system	monoclinic	triclinic	triclinic	triclinic	triclinic	triclinic	triclinic	monoclinic
Space group	$P2_1/c$	$P\bar{1}$	$P\bar{1}$	$P\bar{1}$	$P\bar{1}$	$P\bar{1}$	$P\bar{1}$	$C2/m$
a (Å)	16.951(4)	9.450(3)	9.462(2)	10.379(2)	10.575(1)	10.107(1)	10.200(1)	8.887(6)
b (Å)	14,594(4)	10.965(3)	10.899(2)	11.008(3)	11.538(1)	13.089(1)	13.020(2)	25.053(2)
c (Å)	17.472(4)	12.524(4)	13.354(3)	11.165(2)	12.150(1)	13,669(1)	14.065(2)	10.039(7)
α (°)	90	89.565(7)	98.582(4)	66.507(4)	103.246(2)	97.074(1)	95.320(2)	90
β (°)	98.722(6)	72.551(8)	99.984(4)	82.540(4)	95.911(3)	109.843(1)	110.326(3)	101.565(1)
γ (°)	90	79.820(7)	103.542(3)	76.892(4)	92.019(2)	95.596(2)	94.655(3)	90
V (Å^3)	4272.3(2)	1217.1(6)	1292.5(4)	1138.3(4)	1432.8(3)	1669.2(2)	1731.3(4)	2190(3)
Z	4	2	2	2	2	2	2	4
D_{calcd} (g cm^{-3})	1.952	1.812	1.778	2.097	1.755	1.733	1.740	1.850
μ (mm^{-1})	2.784	2.241	2.115	2.634	2.095	1.815	1.754	2.710
F(000)	2392	652	684	698	742	866	902	1156
Total/independent reflections	25244/8382	7309/4717	7741/5025	6808/4406	9449/6091	10048/6439	10693/6917	6702/2428
Parameters	487	294	314	300	375	406	544	120
R_{int}	0.0716	0.0174	0.0763	0.0116	0.0862	0.0176	0.0210	0.0350
R^a, $R_w{}^b$	0.0360, 0.0734	0.0313, 0.0702	0.0316, 0.0821	0.0210, 0.0760	0.0527, 0.1431	0.0303, 0.1194	0.0297, 0.0880	0.0342, 0.0789
GOF^c	1.078	1.030	1.026	1.028	1.037	1.022	1.002	1.010

^{a} $R = \Sigma||F_o| - |F_c|| \,/\, \Sigma|F_o|$. ^{b} $R_w = [\Sigma[w(F_o^2 - F_c^2)^2] \,/\, \Sigma w(F_o^2)^2]^{1/2}$. ^{c} GOF $= \{\Sigma[w(F_o^2 - F_c^2)^2]/(n-p)\}^{1/2}$.

In all these cases, DMF molecules were included in the crystal lattices as coordination solvents. This encourages us to further examine whether such isomeric effect could be caused by changing the pH values or ligated solvents of the reaction system. When we tried our best to prepare La(III) complexes without addition of NaOH or using Et_3N to adjusting the pH value, no single crystalline products could be obtained. When DMF was replaced by the other amide-type solvents including DMA, DEF and NMP, crystals of **3** (in DMA/EtOH), **5** (in DEF/EtOH), **6** (in DMA/EtOH) and **7** (in NMP/EtOH) were achieved, where **3** and **5–7** are isostructural to **2** and **4**, respectively. The results indicate that the positional isomeric effect in the formation of these La(III)–tcbdc systems involving dimensionality changes is independent on the amide-type solvents.

The crystals of **1–7** are sensitive to moisture and should be kept under dry air atmosphere or in the mother liquid. They are insoluble in common organic solvents (such as alcohol, acetonitrile, chloroform and DMF), but can be hydrolyzed rapidly in water (> 100 mg mL^{-1}) that is similar to those reported by our group.[46,48] Thus, we also attempted to grow single crystals of **1–7** by the slow evaporation of their water solutions so as to study their structural transformations. However, only crystals of **8** were obtained by slow evaporation of the water solution of **4**. It is worth noting that attempts to directly synthesize complex **8** via hydrothermal reaction of 1,4-H_2tcbdc with La(III) salts were not successful.

Structural description

Crystal structure of 1

Single-crystal X-ray analysis of **1** reveals that it crystallizes in the monoclinic space group $P2_1/c$ and shows 2D layered structure. The asymmetric unit contains two crystallographically independent La(III) ions (La1 and La2), three 1,2-tcbdc ligands, four coordinated water molecules, and two lattice ethanol molecules. The La1 atom is nine-coordinated (LaO_9) and has a distorted tricapped trigonal prism geometry (Scheme 3a), while

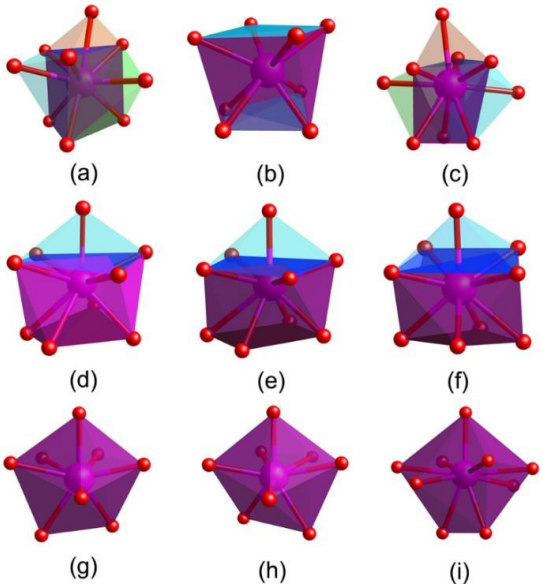

Scheme 3 Diverse coordination geometries (tricapped trigonal prism for a and c, square antiprism for b, mono-capped square antiprism for d–f, dodecahedron for g and h, and tetrakaidecahedron for i) of La(III) ions in complexes **1**–**8**.

the La2 atom is eight-coordinated (LaO_8) in a distorted square antiprism geometry (Scheme 3b). The La–O bond distances are in the range of 2.348(8)–2.690(8) Å, which are in agreement with those reported for La(III) CPs with aromatic carboxylate ligands.[54] The 1,2-tcbdc ligands all adopt a μ_3-bridging mode to connect three La(III) ions, however, they show three types of coordination modes, that is, 1,2-tcbdc^{I} is μ_3-bridging with each carboxylate in a μ_2-η^1:η^1-*syn-anti*-bridging mode (Scheme S1, mode I, ESI†), 1,2-tcbdc^{II} has μ_2-η^1:η^1-*syn-anti*-bridging and μ_2-η^2:η^1-chelating/bridging modes (Scheme S1, mode II, ESI†), and 1,2-tcbdc^{III} displays μ_2-η^1:η^1-*syn-syn*-bridging and chelating fashions (Scheme S1, mode III, ESI†). Thus, the neighbouring LaO_9 polyhedra of La1 share an edge through two carboxylate oxygen atoms from two 1,2-tcbdc^{II} ligands to give a La_2O_{16} dimer with a La···La separation of 4.429(1) Å. These dimmers are further connected with six LaO_8 polyhedra of La2 by eight carboxylate groups from three pairs of 1,2-tcbdc^{I}, 1,2-tcbdc^{II} and 1,2-tcbdc^{III} ligands, forming a 2D network (Fig. 1a), where the tetrachlorinated phenyl rings project on both the sides of the layer (Fig. 1b). From the view point of topology, as depicted in Fig. 1c, such a 2D layer could be described as a unique 4-nodal (3,4,5)-connected net with the Schläfli symbol of $\{4\cdot8^2\}\{4^2\cdot8^4\}\{4^3\}_2\{4^6\cdot8^4\}$, in which the La1 center as a 5-connected node and the La2 center as a 4-connected node as well as each 1,2-tcbdc ligand as a 3-connected linker.

It should be pointed out that there are four crystallographically independent water molecules (O13, O14, O15 and O16) coordinated to the La2 center. The $[La(H_2O)_4]$ moieties are further

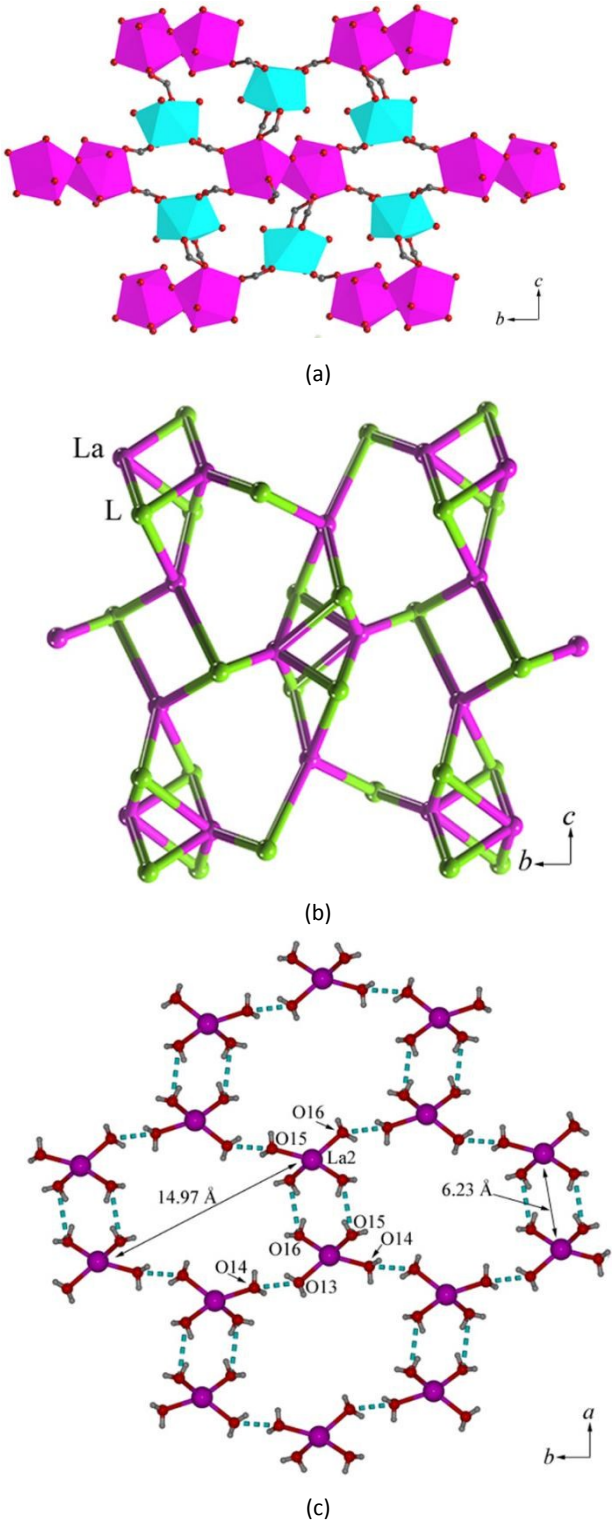

Fig. 1 Crystal structure of **1**. (a) The 2D layer containing La_2O_{16} dimer and LaO_8 polyhedron viewed along the *bc* plane. (b) A schematic representation of the 2D (3,4,5)-connected network. (c) The 2D water network constructed from $[La(H_2O)_4]$ moieties along the *ab* plane.

connected to each other by hydrogen bonds, resulting in a 2D $[La(H_2O)_4]_n$ sheet along the *bc* plane (Fig. 1d). The H-bonding distances vary from 2.942 to 3.571 Å, which is within the range of 2.3–3.6 Å reported in the literature.[55] The average O···O distance of 3.256 A is comparable to the sum of van der Waals radii 3.2 Å. Such 2D metal-water motif is embedded in the above-mentioned 2D coordination network. In addition, the coordination layers showing a parallel arrangement are connected by Cl···Cl interactions (Cl3···Cl7 distance = 3.505 Å, Cl6···Cl9 distance = 3.465 Å) to generate a 3-D supramolecular network (Fig. S1, ESI†). The Cl···Cl distance is shorter than twice Pauling's van der Waals radius of the Cl atom (3.76 Å),[56] and that stated by Bondi (3.52 Å).[57]

Crystal structures of 2 and 3

When the 1,2-H2tcbdc ligand was replaced by the 1,3-H2tcbdc ligand, we obtained **2** and **3** with similar 1D double chain structures. X-Ray structural determination indicates that **2** and **3** are isostructural (see Table 1), with the only differences being the coordination geometries of La(III) ions (Scheme 3c for **2** and Scheme 3d for **3**) and the coordinated carbonyl solvents. Herein, only the crystal structure of **2** is described in detail as an example. The asymmetric unit of **2** consists of one La(III) ion, one 1,3-tcbdc anion, one coordinated acetate anion, two coordinated DMF molecules. Each La(III) ion is nine-coordinated and resembles a distorted tricapped trigonal prism geometry. In **2**, each 1,3-tcbdc ligand is in a μ_3-bridging fashion with one carboxylate group displaying a monodentate coordination mode whereas the other exhibiting a μ_2-η^1:η^1-*syn*-*syn*-bridging mode (Scheme S1, mode IV, ESI†), which bridges the La(III) ions to give a binuclear unit. Moreover, such adjacent two La(III) ions are also bridged by two acetate anions, with the La···La separation of 4.269(1) Å. As a consequence, the La(III) ions are extended by the 1,3-tcbdc linkers to result in 1D double chains along the *b* axis (Fig. 2a). These adjacent 1D arrays are linked by O9–H9B···O5 (H···O/O···O distance: 2.065/2.725(7) Å, angle: 134.1(3)°) hydrogen bonds between the water ligands and acetate anions to form a 2D sheet (Fig. S2, ESI†). These sheets are further extended via comparable C12–H12C···Cl1 (H···Cl/C···Cl distance: 2.858/3.565(1) Å, angle: 131.3°) and C15–H15A···Cl3 (H···Cl/C···Cl distance: 2.862/3.662(1) Å, angle: 141.1°) interactions to form a 3D supramolecular network (Fig. S3, ESI†). Although the basic 1D coordination chains of **2** and **3** are similar, their supramolecular architectures are found to be quite different. In the case of **3**, interchain C14–H14A···Cl3 (H···Cl/C···Cl distance: 2.801/3.427(1) Å, angle: 123.8°) interactions interlink the 1D coordination motifs to afford a 2D supramolecular sheet (Fig. S4, ESI†).

Crystal structures of 4–7

The 1,4-H_2tcbdc ligand was selected to react with La(III) in different solvents under the similar solvothermal conditions, leading to the formation of complexes **4–7** with similar 3D **pcu** topological frameworks based on dinuclear secondary building

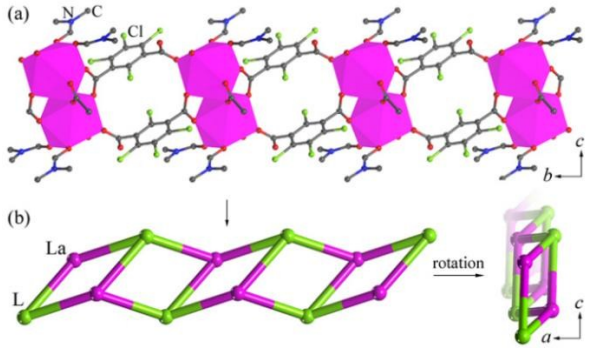

Fig. 2 Crystal structure of **2**. (a) The 1D double chain arrangement along the *b* axis. (b) A schematic representation of the 1D network.

units. In the structure of **4**, each La(III) ion is nine-coordinated (LaO_9) and exhibits mono-capped square antiprism geometry (Scheme 3e). In **4**, the 1,4-tcbdc ligands show two types of coordination modes, that is, 1,4-tcbdc^{I} is μ_4-bridging with each carboxylate group in a μ_2-η^2:η^1-chelating/bridging mode (Scheme S1, mode V, ESI†) and 1,4-tcbdc^{II} is μ_2-bridging with each carboxylate group in a monodentate mode (Scheme S1, mode VI, ESI†). Such a μ_2-η^2:η^1-chelating/bridging mode of the carboxylate group leads to the formation of a dinuclear unit with the La···La distance of 4.502(1) Å. Each dinuclear unit is spanned by four tetrachlorophenyl skeletons from two 1,4-tcbdc^{I} and two 1,4-tcbdc^{II} ligands to form a 2D sheet along the *ac* plane (Fig. 3a).

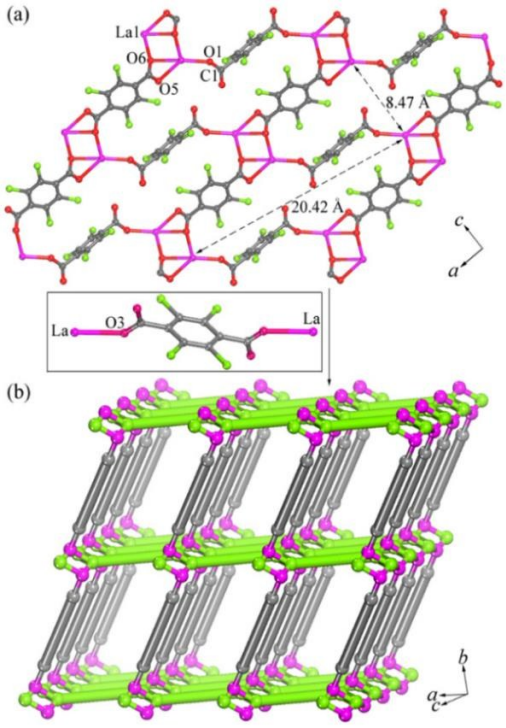

Fig. 3 Crystal structure of **4**. (a) The 2D coordination sheet based on dinuclear units along the *ac* plane. (b) A schematic representation of the 3D coordination framework.

These parallel sheets are further connected by the 1,4-tcbdc^{II} ligands along the *b* axis to form a 3D framework (Fig. 3b) with 6-connected **pcu** net ($4^{12}\cdot6^3$ topology). *PLATON*[49] calculation suggests that neither guest molecules nor an accessible open void is presented in the lattice due to the existence of obstructive chlorine and terminal DMF entities. There exist weak O8–H8A···Cl3 (H···Cl/O···Cl distance: 2.751/3.337(5) Å, angle: 129°) and O9–H9B···Cl1 (H···Cl/O···Cl distance: 2.811/3.485(5) Å, angle: 141°) interactions as well as strong Cl···Cl interactions (Cl4···Cl5 distance = 3.426 Å) (Fig. S5, ESI†).

Similar to **4**, the La(III) ion in **5** is also nine-coordinated (LaO_9) and has a distorted mono-capped square antiprism geometry (Scheme 3f). However, in contrast to **4**, the 1,4-tcbdc ligands in **5** show three types of connectivities, where 1,4-tcbdc^{I} is μ_4-bridging with each carboxylate group in a μ_2-η^2:η^1-chelating/bridging mode (Scheme S1, mode V, ESI†), 1,4-tcbdc^{II} is μ_4-bridging with each carboxylate group in a μ_2-η^1:η^1-*syn-syn*-bridging mode (Scheme S1, mode VI, ESI†), and 1,4-tcbdc^{III} is μ_2-bridging with each carboxylate group in a monodentate mode (Scheme S1, mode V, ESI†). The adjacent La(III) ions are bridged by carboxylate groups to dinuclear units with the La···La distance of 4.235(1) Å, which are further connected to each other through six 1,4-tcbdc^{I} linkers, resulting in a similar 6-connected 3D network to that for **4**. The 3D framework of **5** has very small voids which comprises 4.4% of the unit cell volume as calculated by *PLATON*[49], and thus no guest molecules are included. In addition, Cl4 and Cl5 atoms form intermolecular C14–H14B···Cl4 (H···Cl/C···Cl distance: 2.755/3.652(3) Å, angle: 150°) and intramolecular O1W–H1WC···Cl5 (H···Cl/O···Cl distance: 2.734/3.545(1) Å, angle: 160°) hydrogen bonds with the DEF ligands and coordinated water molecules (Fig. S6, ESI†), falling in the normal range of weak hydrogen bond interactions. Intermolecular Cl···Cl interactions (Cl1···Cl6 distance = 3.537 Å) are also observed.

Complexes **6** and **7** are isostructural except for the differences in the coordination geometries of La(III) ions and the carbonyl solvents. The 3D coordination frameworks of **6** and **7** are also similar to those of **4** and **5**. However, in contrast to the nine-coordinated La(III) ions in **4** and **5**, the La(III) ions in **6** and **7** are eight-coordinated (LaO_8) and display a distorted dodecahedral geometry (Scheme 3g for **6** and Scheme 3h for **7**) due to the presence of larger steric hindrance from the carbonyl groups of DMA and NMP. The coordination modes of 1,4-tcbdc are similar to that of **4**, and the chelating/bridging mode of carboxylate leads to the formation of a dimeric unit with the La···La distances of 4.431(1) and 4.384(1) Å for **6** and **7**, respectively. Notably, although an analysis of the host voids shows that there exists no void space in the crystal structures of **6** and **7** if calculated with the lattice DMA and NMP molecules, after the removal of these guest molecules, the empty spaces comprise 21.1% and 19.3% of the unit cell volumes for **6** and **7**, respectively. Further investigation on their crystal structures indicates that DMA in **6** and NMP in **7** have obvious hydrogen bonding interactions with the whole structures. As for **6**, the coordinated and lattice DMA molecules are involved in intermolecular C15–H15B···Cl4 (H···Cl/C···Cl distance: 2.817/3.687(1) Å, angle: 151°) and C23– H23A···Cl5 (H···Cl/C···Cl distance: 2.973/3.889(1) Å, angle: 160°) interactions with the Cl4 and Cl5 atoms, respectively (Fig. S7, ESI†). In the case of **7**, one coordinated NMP ligand is engaged inC14–H14A···Cl4 (H···Cl/C···Cl distance: 3.024/3.826(1) Å, angle: 141°) and C14–H14B···Cl5 (H···Cl/C···Cl distance: 2.885/3.779(9) Å, angle: 126°) hydrogen bonding with the Cl4 and Cl5 atoms, while the lattice NMP guests are incorporated into the host framework via C26–H26B···O4#1 (H···O/C···O distance: 2.653(1)/3.617(9) Å, angle: 172°) interactions with the aqua ligands (Fig. S8, ESI†).

Crystal structure of 8

In contrast to the solvothermal synthetic routes for **4–7**, complex **8** based on 1,4-tcbdc was obtained by slowly evaporating the water solution of the as-synthesized **4** at room temperature, giving structural transformation from 6-connected 3D framework

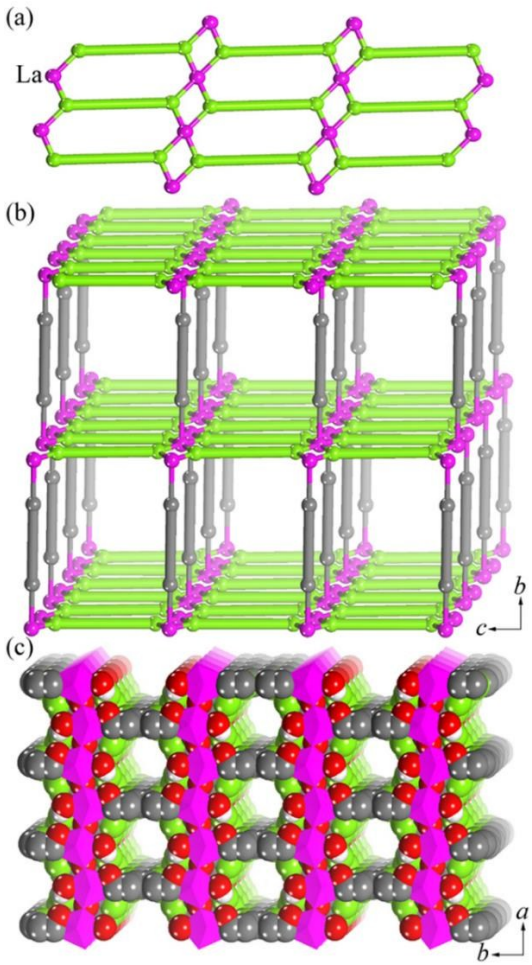

Fig. 4 Crystal structure of **8**. (a) The 2D coordination sheet constructed from 1,4-tcbdc^{I} ligands. (b) A schematic representation of the 3D 4,5-connected network. (c) The 3D coordination framework viewed along the *c* axis.

Table 2 Positional isomeric effect and solvent effect in complexes **1–7**

complex	ligand	crystallizing medium	metal geometry	coordination mode of carboxylate	coordination network
1	1,2-H_2tcbdc	DMF/EtOH	Scheme 3a and 3b (LaO_9 and LaO_8)	μ_2-η^1:η^1-*syn-anti*-bridging, μ_2-η^2:η^1-chelating/bridging, μ_2-η^1:η^1-*syn-syn*-bridging and chelating	2D layer
2	1,3-H_2tcbdc	DMF/EtOH	Scheme 3c (LaO_9)	monodentate and μ_2-η^1:η^1-*syn-syn*-bridging	1D double chain
3	1,3-H_2tcbdc	DMA/EtOH	Scheme 3d (LaO_9)	monodentate and μ_2-η^1:η^1-*syn-syn*-bridging	1D double chain
4	1,4-H_2tcbdc	DMF/EtOH	Scheme 3e (LaO_9)	μ_2-η^2:η^1-chelating/bridging and monodentate	3D **pcu** net
5	1,4-H_2tcbdc	DEF/EtOH	Scheme 3f (LaO_9)	μ_2-η^2:η^1-chelating/bridging, μ_2-η^1:η^1-*syn-syn*-bridging and monodentate	3D **pcu** net
6	1,4-H_2tcbdc	DMA/EtOH	Scheme 3g (LaO_8)	μ_2-η^2:η^1-chelating/bridging, and monodentate	3D **pcu** net
7	1,4-H_2tcbdc	NMP/EtOH	Scheme 3h (LaO_8)	μ_2-η^2:η^1-chelating/bridging and monodentate	3D **pcu** net

of **4** to 4,5-connected 3D network of **8**. The La(III) ion in **8** is nine-coordinated (LaO_9), but it exhibits a tetrakaidecahedral geometry (Scheme 3i). The 1,4-tcbdc ligands in **8** display two types of connectivities, where 1,4-tcbdc^{I} is μ_4-bridging and the 1,4-tcbdc^{II} is μ_2-bridging. However, different to the bis-monodentate mode for the μ_2-bridging 1,4-tcbdc in **4**, the 1,4-tcbdc^{II} in **8** adopts a chelating bis-bidentate coordination mode (Scheme S1, mode VIII, ESI†). Each 1,4-tcbdc^{I} ligand bridges four La(III) ions and each La(III) ion connects four 1,4-tcbdc^{I} ligands, leading to the formation of a 2D layer (Fig. 4a), which is different to that of **4**. The 1,4-tcbdc^{II} ligand can also act as a bridge to pillar the neighbouring layers to generate a 3D open framework having 1D square-shaped channels with a cross-section of ca. 14.8 × 14.8 Å^2 along the *a* axis, as indicated in Fig. 4b. The channel interior isdecorated with chlorine groups of 1,4-tcbdc ligands (Fig. 4c), where intermolecular Cl···Cl interactions (Cl1···Cl3 distance = 3.412 Å and Cl2···Cl3 distance = 3.521 Å) are observed (Fig. S9, ESI†). The lattice water molecules fill in the chlorous channel of the framework. From a topological perspective, if each La(III) center is regarded as a five-connected node while the 1,4-tcbdc^{I} and 1,4-tcbdc^{II} ligands are two- and four-connected, respectively, thus the resulting 3D structure of **8** can be classified as a rare 4,5-connected network with the point symbol of $\{4^4\cdot6^2\}\{4^4\cdot6^6\}$ topology (Fig. 4b).

Positional Isomeric Effect, Solvent Effect and Water-Induced Structural Transformation

By using a series of 1,2-; 1,3-; and 1,4-H_2tcbdc ligands under similar solvothermal reaction conditions, seven La(III)-based nets (see Table 2 for structural features of **1–7**) can be systematically and regularly controlled. Among them, 1,2-; 1,3-;and 1,4-tcbdc suffer the different steric hindrances and two carboxylate groups have 60°, 120° and 180°, respectively. In **1**, the carboxylate groups of 1,2-tcbdc anions display four kinds of coordination modes to link the La(III) centers into a 2D (3,4,5)-connected sheet. For **2** and **3**, La(III) ions are connected by μ_3-bridging 1,3-tcbdc anions via two kinds of coordination modes into a 1D double chain. In the structures of **4–7**, the 1,4-tcbdc anions adopt μ_2- and μ_4-bridging modes connecting the La(III) ions into 3D dinuclear 6-connected **pcu** frameworks. These results indicate that diverse structural topologies of them mainly depend on the positional isomeric character of the tcbdc ligands.

Although the different sizes of the amide-type solvent molecules do not affect the structural dimensionalities of the final networks, they can subtly influence the coordination geometry around the La(III) ion and the coordination mode of carboxylate.Moreover, the size discrepancy of carbonyl solvent molecules (DMF < DEF < DMA < NMP) around the La(III) ions in **4–7** lead to the different shapes of 1D channels in **4–7** (Fig. S10, ESI†). It is observed that the increase in the carbonyl solvent size may cause the enhancement of the void volumes of overall crystal lattices, which is similar to those reported by Wang et al.[58]

Recently, Bertani *et al*., Fernández *et al*. and Desiraju *et al*. reported the effect of non-covalent C–H···Cl and O–H···Cl hydrogen bonding as well as Cl···Cl interactions on the self-assembly of supramolecular architectures.[59–61] In this contribution, each isomeric tcbdc ligand bearing four substituent groups of chlorine also favors the formation of various hydrogen bonding and Cl···Cl contacts (see Table 3 and Fig. S1–S9). In the structures of **2–7**, the coordinated carbonyl solvents and aqua ligands are always involved in the formation of C–H···Cl and O–H···Cl hydrogen bonding interactions. In addition, intermolecular Cl···Cl interactions were observed in the 2D structure of **1** and 3D structures of **4–8**. Thus, both the positional isomeric effect of ligand and the solvent effect play an important role in extending and stabilizing these structural topologies of **1–8**.

It should be noted here that a 3D 6-connected framework of **4**

Table 3 Parameters of D–H···Cl hydrogen bonding and Cl···Cl interactions in the structures of **1**–**8**

complex	D–H···Cl hydrogen bonding				Cl···Cl interactions	
	D–H···Cl	*d* (H···Cl) / Å	*d* (D···Cl) /Å	∠ D–H···Cl / °	Cl···Cl	*d* (Cl···Cl) /Å
1					Cl3···Cl7#1	3.505
					Cl6···Cl9#1	3.465
2	C12–H12C···Cl1#1	2.858	3.565	131.3		
	C15–H15A···Cl3#2	2.862	3.662	141.1		
3	C14–H14A···Cl3#1	2.801	3.427	123.8		
4	O8–H8A···Cl3#1	2.751	3.337	129.1	Cl4···Cl5#3	3.426
	O9–H9B···Cl1#2	2.811	3.485	141.0		
5	C14–H14B···Cl4#1	2.755	3.652	150.0	Cl1···Cl6#2	3.537
	O1W–H1WC···Cl5	2.734	3.545	160.0		
6	C15–H15B···Cl4#1	2.817	3.687	151.0	Cl2···Cl6	3.366
	C23–H23A···Cl5	2.973	3.889	160.0		
7	C14–H14A···Cl4#1	3.024	3.826	141.0	Cl1···Cl6	3.321
	C14–H14B···Cl5	2.885	3.779	126.0	Cl2···Cl4#1	3.488
8					Cl1···Cl3#1	3.412
					Cl2···Cl3#2	3.521

Symmetry codes for **1**: #1 = –*x*, –*y*, –*z* + 1; For **2**: #1 = –*x*, –*y* + 1, –*z* + 1; #2 = –*x* + 1, –*y*, –*z* + 1; for **3**: #1 = *x* + 1, *y* + 1, *z*; for **4**: #1 = –*x*, –*y*, –*z* + 1; #2 = –*x*, –*y* + 1, –*z*; #3 = –*x*, –*y* + 1, –*z* + 1; for **5**: #1 = –*x* + 1, –*y* + 2, –*z*; #2 = –*x* – 1, –*y* + 1, –*z*; for **6**: #1 = –*x* + 3, –*y* + 1, –*z* + 1; #2 = –*x* +1, –*y*, –*z* + 1; for **7**: #1 = –*x* + 1, –*y*, –*z* + 2; for **8**: #1 = *x* + 1/2, –*y* + 1/2, *z*; #2 = –*x* + 1, –*y*, –*z* + 2.

Table 4 A comparison of the structural transformation upon hydrolysis and reformation in the related compounds

CP precursor	resulting compound	structural transformation	Ref
$[Zn_2Na_2(1,4\text{-tcbdc})_3(DMF)_4(MeOH)]_n$ [a]	$[Zn(H_2O)_6]\cdot(1,4\text{-tcbdc})\cdot 4H_2O$	from 3D to discrete	46
$[Cd_3(1,4\text{-tfbdc})_3(DMF)_2(MeOH)_6]_n$ [b]	$\{[Cd_4(1,4\text{-tfbdc})_4(H_2O)_{11}]\cdot 3.5H_2O\}_n$	from 3D to 1D	46
$\{[Ca_4(1,4\text{-tfbdc})_4(H_2O)_4]\cdot 4H_2O\}_n$ [b]	$[Ca(1,4\text{-tfbdc})(H_2O)_4]_n$	from 3D to 2D	48
$[La(1,4\text{-tcbdc})_{1.5}(DMF)(H_2O)_3]_n$ [a]	$\{[La(1,4\text{-tcbdc})_{1.5}(H_2O)]\cdot 3H_2O\}_n$	from 3D to 3D	this work

[a] 1,4-tcbdc stands for 2,3,5,6-tetrachloro-1,4-benzenedicarboxylate. [b] 1,4-tfbdc is 2,3,5,6-tetrachloro-1,4-benzenedicarboxylate.

was found to convert to a new 3D 4,5-connected framework of **8**. Combined with our previously reported water-induced structural transformations including the changes from 3D metal-organic frameworks of Zn(II), Cd(II) and Ca(II) to discrete ion-pair structure, 1D chain, and 2D layer (see Table 4), it is strongly suggested that water-soluble La(III) CPs can undergo hydrolysis and recrystallization in water and tend to form high-dimensionality network structures because the La(III) ions generally possess larger radii and higher coordination numbers. On the other hand, since complex **8** could not be obtained directly by the reaction of 1,4-H_2tcbdc with La(III) salts in water, it might be expected that water-soluble lanthanide complexes can server as precursors to produce new high-dimensional frameworks.

Powder X-ray diffraction and thermal stability analyses

In order to confirm the phase purity of the bulk materials, powder X-ray diffraction (PXRD) experiments were carried out for complexes **1**–**8** at room temperature. As shown in Fig. S11 (ESI†), the peak positions of simulated and experimental PXRD patterns at room temperature are in agreement with each other, indicative of pure products. The dissimilarities in intensity may be attributed to the preferred orientation of these crystalline powder samples. To further estimate the thermal stability of the eight complexes, their thermal behaviors were

investigated by thermogravimetric (TG) analyses (Fig. S12, ESI†). The TG results show that the coordination frameworks of **1**, **4** and **8** are more stable than the others. It seems that the formation of 3D frameworks of **4**–**8** do not always enhance its thermal stability as compared with the other 1D and 2D complexes.

Ring-Opening Polymerization of glycolide

Poly(glycolic acid) (PGA) is one of the leading sustainable materials for their biomedical applications in orthopaedics.[62] The most efficient synthesis, and the commercial route to PGA, involves the ring-opening polymerization (ROP) of the cyclic diester glycolide. In recent years, lanthanide complexes have proven to be efficient initiators for the ROP of cyclic monomers such as lactide and *ε*-caprolactone.[32–36]. Moreover, most of catalysts for ROP are just limited in the solution polymerization. Up to date, few report of their use for the bulk polymerization has been documented. [63] To our knowledge, there has been no report concerning the application of lanthanide complexes for the ROP of glycolide.

The solid-state bulk polymerization is the key for the fabrication of high-molecular-weight PGA without any organic solvents, where the melt/solid polycondensation of glycolide generally occurs in the temperature of 180–230 °C.[64] Such reaction processes are very fast, and PGA samples can be analyzed by isothermal DSC. In this work, the bulk solvent-free melt ROP of glycolide was carried out by employing the as-synthesized complexes **1**–**8**, and the influence of topological structures on the catalytic activity was studied.

In the isothermal DSC polymerization of glycolide, the measured heat is totally generated from the ROP of glycolide, and the total peak area of DSC curve is proportional to the heat. The polymerization rate of glycolide is proportional to the heat flow with the following equation.

$$\frac{da}{dt} = \frac{dH}{dt}\ \frac{1}{\Delta H} \qquad (1)$$

Where ΔH is the total heat during the entire polymerization, $\frac{dH}{dt}$ represents the measured heat flow, and $\frac{da}{dt}$ is the polymerization rate. Meanwhile, the measured heat flow, $\frac{dH}{dt}$, is proportional to the polymerization rate, which can be obtained by differentiating α with respect to *t*, as expressed by equation (2).

$$\frac{da}{dt} = k(T)f(cat)f(a) \qquad (2)$$

Where $k(T)$ is the reaction rate constant, $f(cat)$ is the concentration dependent function of catalyst, and $f(a)$ is the concentration dependent function of glycolide monomer. The dependence of $k(T)$ on temperature can be given by Arrhenius expression.

$$k(T) = k_0 \exp(-\frac{E_a}{RT}) \qquad (3)$$

Where E_a is the activation energy, k_0 is the frequency factor, T is the Kelvin temperature, and R is the universal gas constant.

Table 5 DSC data for the polymerization of glycolide initiated by complexes **1**–**8**[a]

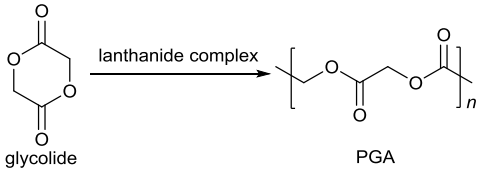

initiator	temp (°C)	ln(1−α)[b]	n[b]	K[b] ($S^{-1}\times10^{-3}$)	E_a[b] (kJ mol^{-1})
1	200	–0.45	0.71	5.26	18.87±
1	205	–0.36	0.83	6.06	2.21
1	210	–0.43	0.79	5.93	
1	215	–0.40	0.80	6.41	
1	220	–0.39	0.82	6.79	
2	200	8.58	1.08	4.89	54.68±
2	205	8.61	1.17	5.83	3.87
2	210	8.71	1.20	7.43	
2	215	8.64	1.24	7.96	
2	220	8.69	1.27	9.60	
3	200	14.82	1.44	7.62	77.50±
3	205	15.23	1.80	14.00	6.38
3	210	15.03	1.60	14.00	
3	215	15.00	1.57	17.00	
3	220	14.89	1.55	18.00	
4	200	–0.87	0.32	2.13	20.78±
4	205	–0.86	0.36	2.27	2.49
4	210	–0.73	0.57	2.73	
4	215	–0.77	0.58	2.77	
4	220	–0.62	0.73	3.89	
5	200	5.00	0.86	13.00	36.68±
5	205	4.95	0.70	14.00	3.92
5	210	5.00	0.82	16.00	
5	215	4.96	0.75	17.00	
5	220	5.03	0.90	20.00	
6	200	26.40	0.95	3.67	125.56
6	205	26.48	0.79	5.57	±14.79
6	210	26.45	0.66	7.47	
6	215	26.15	0.57	7.68	
6	220	26.19	0.65	11.00	
7	200	25.92	0.52	2.86	125.02
7	205	26.19	0.89	5.20	±8.68
7	210	26.35	1.03	8.48	
7	215	26.40	1.06	12.00	
7	220	26.27	1.12	15.00	
8	200	1.24	0.43	2.39	28.63±
8	205	1.32	0.57	2.79	4.58
8	210	1.31	0.64	2.98	
8	215	1.44	0.75	3.65	
8	220	1.39	0.68	3.72	

[a] Each reaction was performed in melt at different reaction temperature with a glycolide : lanthanide complex molar ratio of 4000 : 1. [b] The data were determined by DSC measurement.

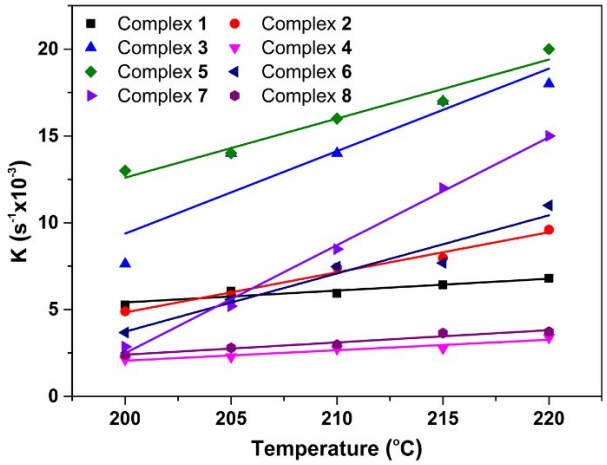

Fig. 5 Plots of rate constant vs reaction temperature for ROP of glycolide catalysed by **1**–**8**.

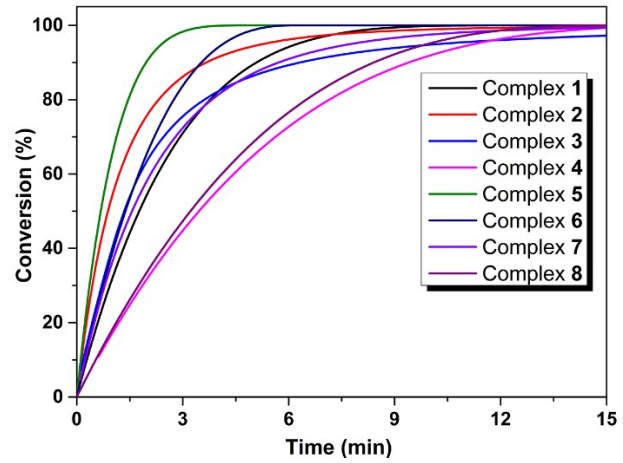

Fig. 6 Plots of conversion of glycolide vs reaction time with **1**–**8** as initiators at 210 °C.

During the ROP of glycolide, the reaction rate is proportional to the concentration of unreacted monomer. Therefore, $f(a)$ can be given by equation (4).[62]

$$f(a) = (1-a) \quad (4)$$

Assuming that the growing species have the same catalytic activities with that of La(III) complexes throughout the polymerization, $f(cat)$ can be given by equation (5).

$$f(cat) = [C_{cat}]^n \quad (5)$$

Where *n* is the reaction order.

Combining equation (1)–(5), the polymerization rate can be described by the following equation.

$$\frac{da}{dt} = k(T)[C_{cat}]^n(1-a) = k_0\exp(-\frac{E_a}{RT})[C_{cat}]^n(1-a) = K(T)(1-a) \quad (6)$$

Where $K(T)$ is the apparent polymerization rate constant, as given by equation (7).

$$K(T) = k(T)[C_{cat}]^n = k_0\exp(-\frac{E_a}{RT})[C_{cat}]^n \quad (7)$$

From equation (6), the following equation can be obtained, which can be used to determine $K(T)$.

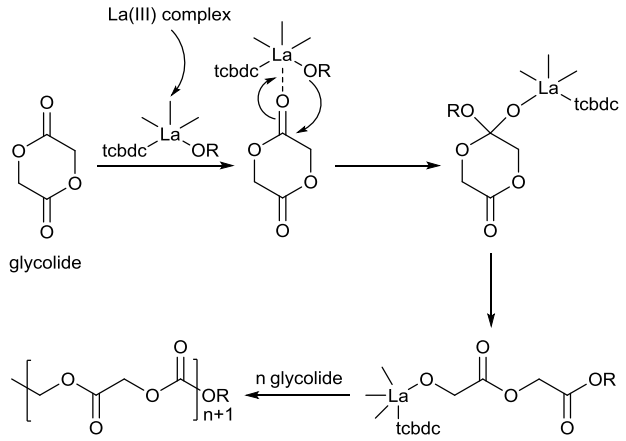

Scheme 4 Proposed mechanism for the ROP of glycolide by La(III) complexes.

$$\ln(1-a) = K(T)(t-t_0) \quad (8)$$

Where t_0 is the time delay in DSC polymerization.

The representative polymerization data are summarized in Table 5. It was found that all the La(III) complexes could initiate the ROP of glycolide with the kinetic reaction orders ranging from 0.32 to 1.80 in the range 200–220 °C. The reaction rate constant on reaction temperature in Fig. 5 revealed that these bulk polymerizations at higher temperature are relatively faster, which is also consistent with their enthalpy changes. Complexes **3** and **5** exhibited comparatively higher catalytic activity than the other complexes. The catalytic activity decreased in the order **5** > **3** > **7** > **6**> **2** > **1** > **8** > **4** (> 215 °C). Furthermore, by investigating the relationship between conversion and reaction time at 210 °C (Fig. 6), the conversion of glycolide could be completed within 15 min.

On the basis of the above experimental results and previous

Table 6 Polymerization of glycolide catalysed by complexes **1**–**8**[a]

initiator	M_n[b]	M_w[b]	M_w/M_n[b]
1	39350	75160	1.91
2	55523	93280	1.68
3	94524	117210	1.24
4	18415	39410	2.14
5	103987	122705	1.18
6	58850	97103	1.65
7	70802	104079	1.47
8	20065	41937	2.09

[a] Each reaction was performed with the lanthanide complex molar ratio of 4000 : 1 at 210 °C for 60 min. [b] Determined by GPC analysis in 1,1,1,3,3,3-hexafluoro-2-propanol calibrated with standard poly(methyl methacrylate).[a]

literature,[66–71] one possible reaction mechanism for the present ROP of glycolide is shown in Scheme 4. The monomer glycolide is coordinated to the La(III) center at the first stage, forming an alkoxyl lanthanide species.[37] Then, the chain propagation process was performed through a coordination-insertion process. The different catalytic activity for **1**–**8** might be caused by the difference in their coordination environments of the La(III) center. In this context, the positional isomeric effect of ligand tcbdc and the solvent effect play a critical role in determining the coordination geometry and steric hindrance around the La(III) ion and thus controlling over the initiation and propagation step.

Since the bulky polymerization can afford high molecular weight polyesters, the polymerization of glycolide initiated by complexes 1–8 was carried out under the same conditions (see Table 6). It was found that the molecular weights (M_n) of the resultant PGA are in the range 84337 – 122705 g mol^{-1} and the molecular weight distributions (M_w/M_n) range from 1.18 to 2.14. Notably, the initiators 3, 5 and 7 showed high activity towards glycolide polymerization, giving the PGA with high molecular weight (M_n > 120000 g mol^{-1}) and quite narrow molecular-weight distributions (1.18 < M_w/M_n < 1.47). The results indicated that the three complexes may serve as potential initiators for the preparation of high molecular weight polyesters

Conclusions

Eight new La(III) coordination polymers have been prepared by the employment of three positional isomers of 1,2-; 1,3-; and 1,4-H_2tcbdc ligands. The network structures of **1–7** are directed by the positions of carboxyl groups on tcbdc backbones, resulting in 2D (3,4,5)-connected sheet for **1**, 1D double chain for **2** and **3**, and 3D 6-connected **pcu** net for **4–7**, respectively. The effect of the sizes of carbonyl solvents (DMF < DEF < DMA < NMP) on the coordination mode of carboxylate, the coordination geometry of La(III) ion, the porous shape and void volume is observed in complexes **4–7**. The crystalline solid of **4** can act as a precursor to produce a new complex **8** by recrystallization in water along with a structural transformation from 3D **pcu** framework to 3D (4,5)-connected net. All Complexes were found to be involved in the efficient initiation of the bulky polymerization of glycolide, and their topological structures have a significant effect on the activity. This work enriches and facilitates the positional isomeric effect of dicarboxylate ligands on the structures and catalytic properties of La(III)-based CPs and further studies involving other metals and ligands are in progress.

Acknowledgements

We gratefully acknowledge financial support by the National Natural Science Foundation of China (21201026 and U1162115), the Nature Science Foundation of Jiangsu Province (BK20131142), and Advanced Catalysis and Green Manufacturing Collaborative Innovation Center—Changzhou University.

References

1 H.-C. Zhou and S. Kitagawa, *Chem. Soc. Rev.*, 2014, **43**, 5415.
2 H.-C. Zhou, J. R. Long and O. M. Yaghi, *Chem. Rev.*, 2012, **112**, 673.
3 J.-R. Li, J. Sculley and H.-C. Zhou, *Chem. Rev.*, 2012, **112**, 869.
4 L. Chen, Q. Chen, M. Wu, F. Jiang and M. Hong, *Acc. Chem. Res.*, 2015, **48**, 201.
5 C. Wang, T. Zhang and W. Lin, *Chem. Rev.*, 2012, **112**, 1084.
6 Y. Cui, Y. Yue, G. Qian and B. Chen, *Chem. Rev.*, 2012, **112**, 1126.
7 W. Zhang and R.-G. Xiong, *Chem. Rev.*, 2012, **112**, 1163.
8 K. Liu, W. Shi and P. Cheng, *Coord. Chem. Rev.*, 2014, **40**, 1760.
9 B. F. Hoskins and R. Robson, *J. Am. Chem. Soc.*, 1990, **112**, 1546.
10 W.-Y. Sun, T. Kusukawa and M. Fujita, *J. Am. Chem. Soc.*, 2002, **124**, 11570.
11 R.-Q. Zhou, H. Sakurai and Q. Xu, *Angew. Chem., Int. Ed.*, 2006, **45**, 2542.
12 Y.-Z. Zheng, M.-L. Tong, W. Xue, W.-X. Zhang, X.-M. Chen, F. Grandjean and G. J. Long, *Angew. Chem., Int. Ed.*, 2007, **46**, 6076.
13 Y.-L. Gai, F.-L. Jiang, K.-C. Xiong, L. Chen, D.-Q. Yuan, L.-J. Zhang, K. Zhou and M.-C. Hong, *Cryst. Growth Des.*, 2012, **12**, 2079.
14 C.-P. Li and M. Du, *Chem. Commun.*, 2011, **47**, 5958.
15 L.-S. Long, *CrystEngComm*, 2010, **12**, 1354.
16 M. Du, C.-P. Li, C.-S. Liu and S.-M. Fang, *Coord. Chem. Rev.*, 2013, **257**, 1282.
17 S. Biswas, H. S. Jena, S. Goswami, S. Sanda and S. Konar, *Cryst. Growth Des.*, 2014, **14**, 1287.
18 S. Parshamoni, S. Sanda, H. S. Jena, K. Tomar and S. Konar, *Cryst. Growth Des.*, 2014, **14**, 2022.
19 S. Biswas, H. S. Jena, A. Adhikary and S. Konar, *Inorg. Chem.*, 2014, **53** 3926.
20 B.-H. Ye, B.-B. Ding, Y.-Q. Weng and X.-M. Chen, *Cryst. Growth Des.*, 2005, **5**, 801.
21 F.-P. Huang, J.-L. Tian, G.-J. Chen, D.-D. Li, W. Gu, X. Liu, S.-P. Yan, D.-Z. Liao and P. Cheng, *CrystEngComm*, 2010, **12**, 1269.
22 Y. Wan, L. Zhang, L. Jin, S. Gao and S. Lu, *Inorg. Chem.*, 2003, **42**, 4985.
23 F. Guo, F. Wang, H. Yang, X. Zhang and J. Zhang, *Inorg. Chem.*, 2012, **51**, 9677.
24 S. Mukherjee, D. Samanta and P. S. Mukherjee, *Cryst. Growth Des.*, 2013, **13**, 5335.
25 M.-L. Han, Y.-P. Duan, D.-S. Li, H.-B. Wang, J. Zhao and Y.-Y. Wang, *Dalton Trans.*, 2014, **43**, 15450.
26 Y.-P. Wu, D.-S. Li, J. Zhao, Z.-F. Fang, W.-W. Dong, G.-P. Yang and Y.-Y. Wang, *CrystEngComm*, 2012, **14**, 4745.
27 G.-P. Yang, Y.-Y. Wang, W.-H. Zhang, A.-Y. Fu, R.-T. Liu, E. K. Lermontova and Q.-Z. Shi, *CrystEngComm*, 2010, **12**, 1509.
28 M. A. Braverman and R. L. LaDuca, *Cryst. Growth Des.*, 2007, **7**, 2343.
29 A. M. Plonka, D. Banerjee and J. B. Parise, *Cryst. Growth Des.*, 2012, **12**, 2460.
30 J. A. Wilson, J. W. Uebler and R. L. LaDuca, *CrystEngComm*, 2013, **15**, 5218.
31 F. T. Edelmann, *Chem. Soc. Rev.*, 2012, **41**, 7657.
32 K. Nie, L. Fang, Y. Yao, Y. Zhang, Q. Shen and Y. Wang, *Inorg. Chem.*, 2012, **51**, 11133.
33 K. Nie, W. Gu, Y. Yao, Y. Zhang and Q. Shen, *Organometallics*, 2013, **32**, 2608.

34 P. Liu, H. Chen, Y. Zhang, M. Xue, Y. Yao and Q. Shen, *Dalton Trans.*, 2014, **43**, 5586.
35 W. Li, M. Xue, J. Tu, Y. Zhang and Q. Shen, *Dalton Trans.*, 2012, **41**, 7258.
36 X. Xu, Z. Zhang, Y. Yao, Y. Zhang and Q. Shen, *Inorg. Chem.*, 2007, **46,** 9379.
37 O. Dechy-Cabaret, B. Martin-Vaca and D. Bourissou, *Chem. Rev.*, 2004, **104**, 6147.
38 F. Coumes, V. Darcos, D. Domurado and S. Li, *Poly. Chem*., 2013, **4**, 3705.
39 F. E. Kohn, J. G. Van Ommen and J. Feijen, *Eur. Polym. J*., 1983, **19**, 1081.
40 S. M. F. Vilela, A. D. G. Firmino, R. F. Mendes, J. A. Fernades, D. Ananias, A. A. Valente, H. Ott, L. D. Carlos, J. Rocha, J. P. C. Tomé and F. A. A. Paz, *Chem. Commun.*, 2013, **49**, 6400.
41 P. Wu, C. He, J. Wang, X. Peng, X. Li, Y. An and C. Duan, *J. Am. Chem. Soc.*, 2012, **134**, 14991.
42 R. Sen, D. Saha and S. Koner, *Catal. Lett*., 2012, **142**, 124.
43 X. Wang, L. Zhang, J. Yang, F. Liu, F. Dai, R. Wang and D. Sun, *J. Mater. Chem. A*, 2015, **3**, 12777.
44 S.-C. Chen, Z.-H. Zhang, K.-L. Huang, Q. Chen, M.-Y. He, A.-J. Cui, C. Li, Q. Liu and M. Du, *Cryst. Growth Des.*, 2008, **8**, 3437.
45 S.-C. Chen, Z.-H. Zhang, Y.-S. Zhou, W.-Y. Zhou, Y.-Z. Li, M.-Y. He, Q. Chen and M. Du, *Cryst. Growth Des.*, 2011, **11**, 4190.
46 S.-C. Chen, Z.-H. Zhang, K.-L. Huang, H.-K. Luo, M.-Y. He, M. Du and Q. Chen, *CrystEngComm*, 2013, **15**, 9613.
47 S.-C. Chen, Z.-H. Zhang, Q. Chen, L.-Q. Wang, J. Xu, M.-Y. He, M. Du, X.-P. Yang and R. A. Jones, *Chem. Commun.*, 2013, **49**, 1270.
48 S.-C. Chen, F. Tian, K.-L. Huang, C.-P. Li, J. Zhong, M.-Y. He, Z.-H. Zhang, H.-N. Wang, M. Du and Q. Chen, *CrystEngComm*, 2014, **16**, 7673.
49 *PLATON* program: A. L. Spek, *Acta Crystallogr., Sect. A*, 1990, **46**, 194.
50 G. M. Sheldrick, *SADABS*, *Program for Empirical Absorption Correction of Area Detector Data*, University of Göttingen, Germany, 1997.
51 Bruker AXS, *SAINT Software Reference Manual*; Madison, WI, 1998.
52 G. M. Sheldrick, *Acta Crystallogr.*, 2008, **A64**, 112.
53 P. V. D. Sluis and A. L. Spek, *Acta Crystallogr.*, 1990, **A46**, 194.
54 S. K. Ghosh and P. K. Bharadwaj, *Inorg. Chem.*, 2005, **44**, 3156.
55 U. S. Raghavender, S. Aravinda, N. Shamala, Kantharaju, R. Rai and P. Balaram, *J. Am. Chem. Soc.*, 2009, **131**, 15130.
56 L. Pauling, *The Nature of the Chemical Bond*, Cornell University, New York, 1960.
57 A. Bondi, *J. Phys. Chem.*, 1964, **68**, 441.
58 W.-H. Huang, G.-P. Yang, J. Chen, X. Chen, C.-P. Zhang, Y.-Y. Wang and Q,-Z. Shi, *Cryst. Growth Des.*, 2013, **13**, 66.
59 R. Bertani, P. Sgarbossa, A. Venzo, F. Lelj, M. Amati, G. Resnati, T. Pilati, P. Metrangolo and G. Terraneo, *Coord. Chem. Rev*., 2010, **254**, 677.
60 C. Rest, M. J. Mayoral, K. Fucke, J. Schellheimer, V. Stepanenko and G. Fernández, *Angew. Chem., Int. Ed.*, 2013, **52**, 1.
61 A. Mukherjee and G. R. Desiraju, *Cryst. Growth Des.*, 2011, **11**, 3735.
62 J. C. Middleton and A. J. Tipton, *Biomaterials*, 2000, **21**, 2335.
63 B. B. Idage, S. B. Idage A. S. Kasegaonkar and R. V. Jadhav, *Mater. Sci. Eng. B*, 2010, **168**, 193.
64 K. Takahashi, I. Taniguchi, M. Miyamoto and Y. Kimura, *Polymer*, 2000, **41**, 8725.
65 J. H. Flynn, *J. Therm. Anal. Calorim.*, 1991, **37**, 293.
66 H. R. Kricheldorf, M. Berl and N. Scharnagl, *Macromolecules*, 1988, **21**, 286.
67 M. Nishiura, Z. Hou, T. A. Koizumi, T. Imamoto and Y. Wakatsuki, *Macromolecules*, 1999, **32**, 8245.
68 H. R. Kricheldorf and I. Kreiser-Saunders, *Polymer*, 2000, **41**, 3957.
69 C. K. Williams, L. E. Breyfogle, S. K. Choi, W. Nam, V. G. Young, Jr., M. A. Hillmyer and W. B. Tolman, *J. Am. Chem. Soc.*, 2003, **125**, 11350.
70 D. Pappalardo, L. Annunziata and C. Pellecchia, *Macromolecules*, 2009, **42**, 6056.
71 D. J. Darensbourg and O. Karroonnirun, *Macromolecules*, 2010, **43**, 8880.